

Strain and interfacial engineering to accelerate hydrogen evolution reaction of two-dimensional phosphorus carbide

Tao Huang(黄韬), Yuan Si(思源), Hong-Yu Wu(吴宏宇), Li-Xin Xia(夏立新), Yu Lan(蓝郁), Wei-Qing Huang(黄维清)†, Wang-Yu Hu(胡望宇), and Gui-Fang Huang(黄桂芳)$

Citation: Chin. Phys. B, 2021, 30 (**2**): 027101. DOI: 10.1088/1674-1056/abbbe7
Journal homepage: http://cpb.iphy.ac.cn; http://iopscience.iop.org/cpb

What follows is a list of articles you may be interested in

Interfacial properties of g-C_3N_4/TiO_2 heterostructures studied by DFT calculations

Chen-Shan Peng(彭春山), Yong-Dong Zhou(周永东), Sui-Shuan Zhang(张虽栓), and Zong-Yan Zhao(赵宗彦)
Chin. Phys. B, 2021, 30 (**1**): 017101. DOI: 10.1088/1674-1056/abb30b

First-principles study of magnetism of 3d transition metals and nitrogen co-doped monolayer MoS_2

Long Lin(林龙), Yi-Peng Guo(郭义鹏), Chao-Zheng He(何朝政), Hua-Long Tao(陶华龙), Jing-Tao Huang(黄敬涛), Wei-Yang Yu(余伟阳), Rui-Xin Chen(陈瑞欣), Meng-Si Lou(娄梦思), Long-Bin Yan(闫龙斌)
Chin. Phys. B, 2020, 29 (**9**): 097102. DOI: 10.1088/1674-1056/ab9741

Electronic structures, magnetic properties, and martensitic transformation in all-d-metal Heusler-like alloys Cd_2MnTM(*TM*=Fe, Ni, Cu)

Yong Li(李勇), Peng Xu(徐鹏), Xiaoming Zhang(张小明), Guodong Liu(刘国栋), Enke Liu(刘恩克), Lingwei Li(李领伟)
Chin. Phys. B, 2020, 29 (**8**): 087101. DOI: 10.1088/1674-1056/ab9739

Ab initio calculations on oxygen vacancy defects in strained amorphous silica

Bao-Hua Zhou(周保花), Fu-Jie Zhang(张福杰), Xiao Liu(刘笑), Yu Song(宋宇), Xu Zuo(左旭)
Chin. Phys. B, 2020, 29 (**4**): 047103. DOI: 10.1088/1674-1056/ab75db

The structural, elastic, and electronic properties of $Zr_xNb_{1-x}C$ alloys from first principle calculations

Sun Xiao-Wei, Zhang Xin-Yu, Zhang Su-Hong, Zhu Yan, Wang Li-Min, Zhang Shi-Liang, Ma Ming-Zhen, Liu Ri-Ping
Chin. Phys. B, 2013, 22 (**10**): 107105. DOI: 10.1088/1674-1056/22/10/107105

Strain and interfacial engineering to accelerate hydrogen evolution reaction of two-dimensional phosphorus carbide*

Tao Huang(黄韬)[1], Yuan Si(思源)[1], Hong-Yu Wu(吴宏宇)[1], Li-Xin Xia(夏立新)[2], Yu Lan(蓝郁)[3], Wei-Qing Huang(黄维清)[1,†], Wang-Yu Hu(胡望宇)[4], and Gui-Fang Huang(黄桂芳)[1,‡]

[1] *Department of Applied Physics, School of Physics and Electronics, Hunan University, Changsha* 410082, *China*
[2] *Department of Physics, Kashgar University, Kashgar* 844006, *China*
[3] *College of Physics and Electronic Engineering, Hengyang Normal University, Hengyang* 421002, *China*
[4] *School of Materials Science and Engineering, Hunan University, Changsha* 410082, *China*

(Received 5 July 2020; revised manuscript received 26 August 2020; accepted manuscript online 28 September 2020)

Hydrogen, regarded as a promising energy carrier to alleviate the current energy crisis, can be generated from hydrogen evolution reaction (HER), whereas its efficiency is impeded by the activity of catalysts. Herein, effective strategies, such as strain and interfacial engineering, are imposed to tune the catalysis performance of novel two-dimensional (2D) phosphorus carbide (PC) layers using first-principle calculations. The findings show that P site in pristine monolayer PC (ML-PC) exhibits higher HER performance than C site. Intriguingly, constructing bilayer PC sheet (BL-PC) can change the coordinate configuration of P atom to form 3-coordination-P atom (3-co-P) and 4-coordination-P atom (4-co-P), and the original activity of 3-co-P site is higher than the 4-co-P site. When an external compressive strain is applied, the activity of the 4-co-P site is enhanced whereas the external strain can barely affect that of 3-co-P site. Interestingly, the graphene substrate enhances the overall activity of the BL-PC because the graphene substrate optimizes the ΔG_{H^*} value of 4-co-P site, although it can barely affect the HER activity of 3-co-P site and ML-PC. The desirable properties render 2D PC-based material promising candidates for HER catalysts and shed light on the wide utilization in electrocatalysis.

Keywords: phosphorus carbide, hydrogen evolution reaction (HER), coordination configuration, electrocatalysis, first principle calculations

PACS: 71.20.–b, 73.20.At, 82.45.Yz **DOI:** 10.1088/1674-1056/abbbe7

1. Introduction

Excessive consumption of fossil fuel makes it urgent to explore alternative sources of energy to substitute fossil fuel or reduce its dependency.[1] Therefore, hydrogen, which is sustainable and environment-friendly, attracts plenty of interests in recent decades.[2] Considered as an effective route to generate hydrogen, the electrocatalytic hydrogen evolution reaction (HER) is the cathodic half-reaction of electrochemical water splitting, where the electrocatalyst is the key to affect the efficiency.[3–6] At present, the noble-metal platinum (Pt) is the most efficient electrocatalyst for HER,[7] which is located near the peak of volcano plots, but the rareness and high cost of Pt hinder the widespread utilization for electrocatalysis.[8,9] Thus, great effort has been made on seeking the nonprecious and highly efficient catalysts to replace the Pt-based materials, such as transition metal phosphides, carbides, borides, nitrides, sulfides and carbon materials, and metal–organic complexes.[10–15]

Most recently, considerable attention has been focused on the HER catalysts based on two-dimensional (2D) materials because of the unique planar structure with atomic thickness and the tunable electronic properties, which can give some obvious advantages for HER catalytic performance.[16,17] For instance, the atomic-thickness structure provides more exposed active sites to facilitate the contact between the reactants and active sites, further permits 2D materials as the ideal platform to facilely interact with other materials or substrates, and makes them easily activated and optimized to obtain higher HER catalytic activity by introducing strain, defects or heteroatoms.

It is reported that 2D transition metal carbides and nitrides (MXenes) have excellent HER performance due to high charge transfer kinetics during the HER with oxygen/hydroxyl termination.[18,19] The 2D triphosphides of GeP_3 and SnP_3, a new class of 2D materials, are theoretically predicted to be highly active for HER with suitable adsorption free energy ΔG_{H^*} in the basal plane.[20–22] As for transition metal dichalcogenides (TMDs), as a representative of 2D material, exhibit high catalytic activity for HER at the edge site and that of the basal plane site can be enhanced by defect modulation, strain engineering or chemical doping.[23–25] What is more, the non-metal catalysts, like g-C_3N_4,[26–29] C_2N,[30,31] and so on, show a potential application in HER with a desired free energy value. Nevertheless, except for the 1T phase of TMDs

*Project supported by the National Natural Science Foundation of China (Grant Nos. 51772085 and U1830138).
†Corresponding author. E-mail: wqhuang@hnu.edu.cn
‡Corresponding author. E-mail: gfhuang@hnu.edu.cn
© 2021 Chinese Physical Society and IOP Publishing Ltd

and most of MXenes, these reported 2D catalysts are semiconductors with poor electrical conductivity.

Attracted a great deal of research interests, graphene has large surface area and excellent conductivity, however, its HER performance is limited by the weak hydrogen adsorption ability on the basal plane.[32] Similarly, phosphorene is promising candidate for HER catalysts for the high carrier mobility, more exposed active sites and tunable electronic properties, but the weak interaction between hydrogen and adsorbed active sites hinder the HER activity.[33,34] Theoretically, the controlled homogenous doping of C (P) in phosphorene (graphene) for the 3-coordinated configuration could generate phosphorus carbide (PC) monolayer.[35] Because of the presence of the non-bonding electron in the C_{2p} orbital, the PC monolayer is metallic, which is ideal for the electrocatalysis HER. However, systematic investigations about HER on layered PC-based materials have not been reported so far.

In this work, a series of investigation is performed to examine the catalytic performance of 2D PC-based materials via first-principle calculation. At first, monolayer PC (ML-PC) and bilayer PC (BL-PC) are constructed and the pristine HER activity of two layered PC materials is examined, which can be descripted by the Gibbs free energy (ΔG_{H^*}). As an effective strategy, external strain is imposed to tune the HER performance. It is interesting that the overall HER activity of BL-PC can be modulated to more desirable at a certain compressive strain. Additionally, H coverage plays a significant role in affecting the HER performance that the higher the coverage is, the lower the HER performance is. The effect of graphene substrate on the catalytic activity is further investigated and the results show that the substrate has a positive effect on the activity of the 4-coordinated-P site but little influence on 3-coordinated-P site of BL-PC and P site of ML-PC. The results provide important guidance for the future development of 2D layered PC materials as excellent metal-free electro-catalysts.

2. Method

The DFT calculations are carried out using the projector augmented wave (PAW) pseudopotentials[36] and the Perdew–Burke–Ernzerhof (PBE) generalized gradient approximation (GGA)[37] for the exchange–correlation functional, as implemented in Vienna *ab-initio* simulation package (VASP) program.[38–40] The cutoff energy for the basis set is chosen to be 500 eV, and the Brillouin zone is sampled with a Γ grid of $5\times5\times1$ for structural optimization and $7\times7\times1$ for density of state calculation. The criterion of convergence is set to 10^{-6} eV for energy and 0.01 eV/Å for force. The vacuum space of 20 Å along the non-periodic directions is set to avoid the interaction between two neighboring layers.

The hydrogen adsorption energy can be computed using the following equation

$$\Delta E_{H^*} = \left(E_{\text{slab}+n\text{H}} - E_{\text{slab}+(n-1)\text{H}} - \frac{1}{2}E_{H_2}\right)/n, \tag{1}$$

where n denotes the number of hydrogen atom adsorbing on the surface, $E_{\text{slab}+n\text{H}}$ and $E_{\text{slab}+(n-1)\text{H}}$ represent the total energies of the studied systems with n and $n-1$ hydrogen atoms on the surface, respectively, and E_{H_2} is the total energy of a hydrogen molecule in the gas phase.

The Gibbs free energies of H^* adsorption can be computed using the following formula:

$$\Delta G_{H^*} = \Delta E_{H^*} + \Delta E_{\text{ZPE}} - T\Delta S, \tag{2}$$

where ΔE_{H^*}, ΔE_{ZPE}, and ΔS are the adsorption energy, zero-point energy change, and the entropy change of H^* adsorption, respectively.[7] In this study, $T\Delta S$ and ΔE_{ZPE} are obtained by the scheme proposed by Norskov *et al.*[3] Specifically, ΔS is calculated using the equation $\Delta S = S_{H^*} - \frac{1}{2}S_{H_2} \approx -\frac{1}{2}S_{H_2}$, in view of the negligible vibrational entropy of H^*. Considering that $TS(H_2)$ is 0.410 eV for H_2 at 298 K and 1 atm (1 atm = 1.01325×10^5 Pa), the corresponding $T\Delta S$ is determined to be -0.205 eV.

3. Results and discussion

Two geometric structures of PC sheet are constructed to investigate the intrinsic catalytic activity of 2D PC material, *i.e.*, monolayer PC and bilayer PC (denoted as ML-PC and BL-PC, respectively). The optimized atomic configuration and electronic properties of ML-PC are examined at first. The original unit cell of monolayer PC is a rectangle lattice with $a = 5.05$ Å and $b = 2.91$ Å.[35,41] In order to attain more possible hydrogen adsorption sites in our work, we change the unit cell lattice from rectangle to a rhombus with the calculated lattice constant is $a = b = 10.03$ Å, as shown in Fig. 1(a). In monolayer PC, every P atom is coordinated with three neighboring C atoms, yielding hexagonal puckered honeycomb configurations with the P atoms located at the outmost atomic layer and the C atoms in the middle atomic layer. Moreover, the P–C bond length is 1.77 Å along the armchair direction and 1.72 Å along the zigzag direction, which is consistent with previous theoretical results.[35] As illustrated in Fig. 2(a), the band structure and partial density of states (PDOS) of ML-PC are calculated to examine the electronic properties of ML-PC. The results show that the ML-PC is metallic and the electronic states near Fermi level are mainly contributed by p-orbitals of P and C atoms, which illustrate a good conductivity for HER.

Three stacking methods to construct bilayer PC structures are considered in our work. Two methods could form van der Waals (vdW) bilayer PC structure (BL-PC), one is simply stacking one ML-PC to another with P and C atoms of

top ML-PC being directly on that of bottom ML-PC, respectively, which is represented by P–P stacking (Fig. A1(a) in Appendix A). The second method is that the C atoms of top ML-PC reside on the P atoms of bottom ML-PC and the P atoms are above the hollow-site of bottom ML-PC, as shown in Fig. A1(b), namely P–C stacking. By stacking one ML-PC on the other reversed ML-PC, the P–P covalent bonds form between the interlayers. Moreover, we calculate the formation energy of three structures to examine the thermodynamic stability. The results show that the formation energy of two vdW bilayer structures is −1.88 eV and −1.94 eV, respectively. Moreover, the formation energy of covalent bond BL-PC is −10.68 eV, indicating that the covalent bond BL-PC is more thermodynamically stable than vdW bilayer structures.

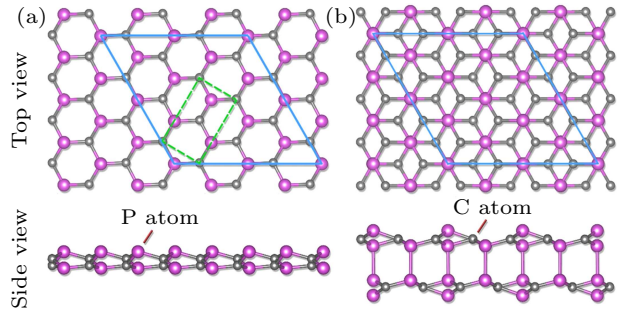


Fig. 1. Optimized atomic configuration of (a) monolayer PC and (b) bilayer PC. The green rectangle represents the original unit cell and the blue rhomb represents the redefined cell. The P and C atoms are denoted as pink and gray spheres, respectively.

The third method is adopted to form a more stable BL-PC structure and the properties are investigated. After fully optimizing, the shape of unit cell remains rhombus with the lattice constant of 10.10 Å, as displayed in Fig. 1(b). It is noteworthy that there are two types of P atoms: one is that P atom bonds to three neighboring C atoms with P–C bond length of 1.77 (1.74) Å along armchair (zigzag) direction, forming 3-coordinated-P atoms (simplified as 3-co-P); the other is the 4-coordinated-P atom (simplified as 4-co-P), which coordinates with three neighboring C atoms and one P atom, and the P–P bond length is 2.34 Å, as shown in Fig. 3(b). The electronic structure of BL-PC is studied by computing the band structure and PDOS (Fig. 2(b)). Different from ML-PC, the BL-PC is a narrow gap semiconductor with a direct bandgap of 0.06 eV. It is shown in Fig. 2(b2) that the states of conduction band minimum (CBM) and valence band maximum (VBM) are contributed by p-orbital of P and C atoms.

Generally, the change in Gibbs free energy of adsorbed H (ΔG_{H^*}) is used as a descriptor to evaluate the intrinsic catalytic activity.[3,7] According to the Sabatier principle,[42,43] the optimal HER catalytic activity occurs when H binding on the surface of reactive intermediates is thermally neutral, *i.e.*, the Gibbs free energy of H* is zero. Therefore, the closer the ΔG_{H^*} is to zero, the better the HER activity is. The HER activity of ML-PC is examined at first and the P and C atoms of ML-PC are considered as active sites for adsorbing H atom (Fig. 3(a)). The calculated free energy value of the P site in ML-PC is −0.05 eV, which is comparable to that of Pt (−0.09 eV). The ΔG_{H^*} value of C site is −0.57 eV, as shown in Fig. 3(c), demonstrating that the interaction between H atom and C site is too strong to desorb and the P site is more active than C site. For comparison, the 3-co-P site and 4-co-P site are considered in BL-PC (Fig. 3(b)). Intriguingly, the values of ΔG_{H^*} suggest that the HER activity of 3-co-P site in pristine BL-PC (−0.14 eV) is comparable to that of P site in ML-PC, which is superior to the 4-co-P site (0.30 eV) in BL-PC for the free energy value closer to zero, which means that the H atom adsorbed on 3-co-P site can be easily desorbed and it is hard for H atom to adsorb on 4-co-P site.

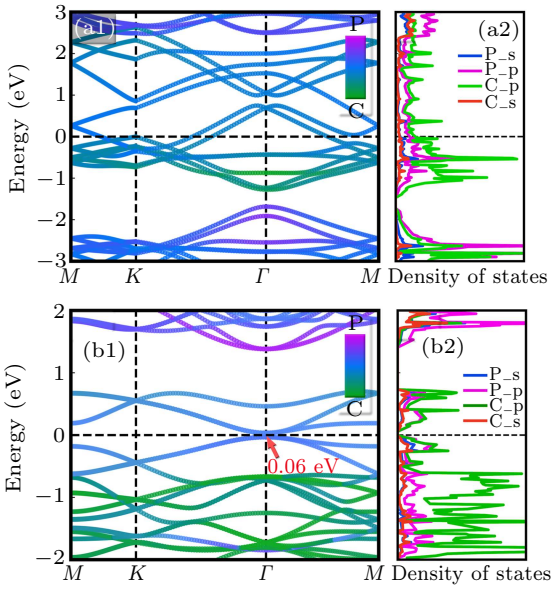


Fig. 2. Band structure and partial density of states (PDOS) of (a) monolayer PC and (b) bilayer PC. The fermi level is set to zero.

Regarded as an effective strategy to modulate the electronic properties of 2D materials, strain engineering may have an influence on HER performance as well.[44,45] To optimize the ΔG_{H^*} of two-layered PC materials, different biaxial strain (ε) parallel to the surface are imposed, which can be defined as $\varepsilon = \Delta a/a_0$, where a_0 is the unstrained lattice parameter and $\Delta a + a_0$ is the strained parameter. As illustrated in Fig. 3(d), the external strain from −2.5% to 2.5% is applied on the ML-PC and BL-PC with an H atom adsorbed on P site, 3-co-P site, and 4-co-P site, respectively. When a tensile strain is applied on the ML-PC, the ΔG_{H^*} value varies slightly from −0.05 eV to 0.004 eV, meaning that the tensile strain can barely affect the excellent HER activity of P site. However, the ΔG_{H^*} value decreases as the applied compressive strain increase and the ΔG_{H^*} value changes to −0.43 eV with the compressive strain reaching −2.5%, inducing a strong interaction between adsorbed H atom and ML-PC catalyst. As for the BL-PC with an applied external strain, the evolution of ΔG_{H^*} value of 3-co-P site exhibits a steady tendency, demonstrating that the

change of external strain could barely influence the catalytic activity of 3-co-P site with an H atom adsorbed on it. Additionally, the ΔG_{H^*} value of 4-co-P site increases monotonously to 0.59 eV with the tensile strain increase to 2.5%. When the applied compressive strain increases, the ΔG_{H^*} of the 4-co-P site shows a general downward trend and the ΔG_{H^*} can be modulated to about zero at a compressive strain of −1.5%. It is worth noting that different from the activity of the 3-co-P site, the catalytic activity of the 4-co-P site is quite sensitive to the external strain and can be optimized by the compressive strain whereas reduced by the tensile strain. Therefore, a certain compressive strain could modulate the overall activity for HER of BL-PC to be more excellent for the ΔG_{H^*} of 3-co-P and 4-co-P site closer to zero simultaneously.

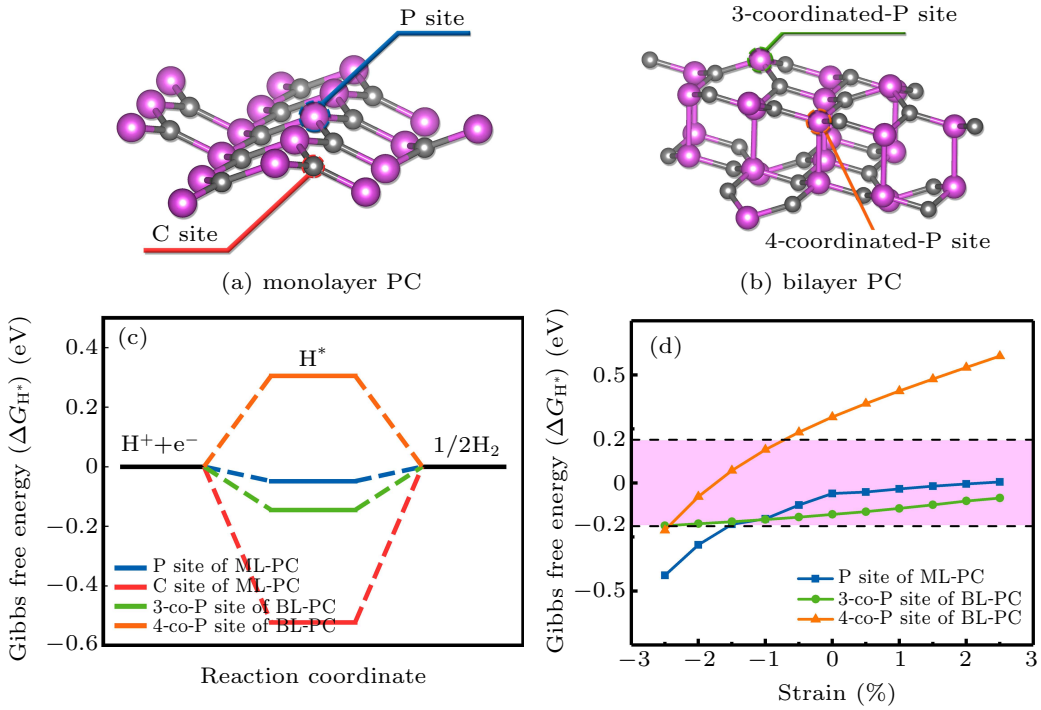


Fig. 3. Schematic view of possible adsorption sites of hydrogen on (a) monolayer PC and (b) bilayer PC sheet. (c) Calculated free energy diagram of hydrogen evolution reaction on different adsorption sites. (d) The ΔG_{H^*} of different active sites as a function of the applied external strain.

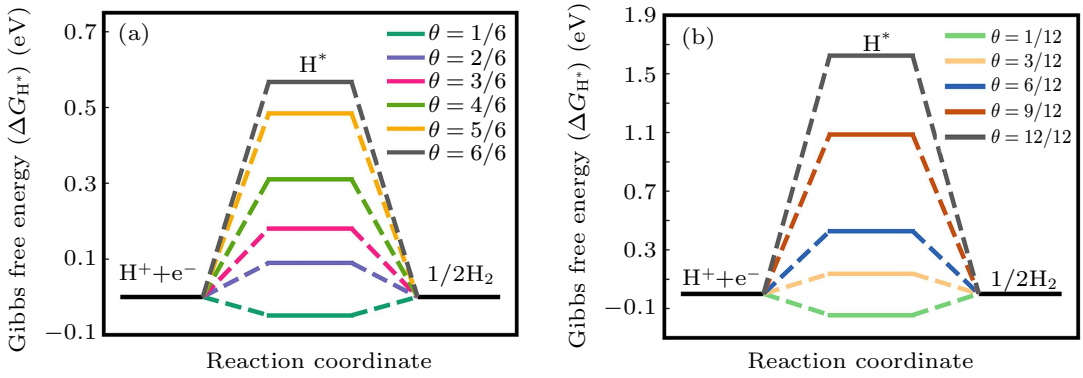


Fig. 4. Calculated free energy diagram of hydrogen evolution reaction at different coverages of (a) monolayer PC and (b) bilayer PC.

A series of calculations are next performed to investigate the evolution of ΔG_{H^*} at different hydrogen coverage (θ). Generally, the hydrogen coverage (θ) is defined as n/N, where$n$ is the number of adsorbed H atoms on the surface and N is the number of active sites of the monolayer. Because of the puckered structure of ML-PC, we consider the top P atoms as active sites so that the number of active sites (N) is 6. The calculated corresponding ΔG_{H^*} with θ ranging from 1/6 to 6/6 of ML-PC are depicted in Fig. 4(a). The results show that as the hydrogen coverage increases, the ΔG_{H^*} increases from −0.05 eV to 0.57 eV, indicating that the interaction between the H atoms and P site is weakened with the number of H atoms adsorbed on surface increasing. At the hydrogen coverage of $\theta = 2/6$ and $\theta = 3/6$, the corresponding free energy is 0.09 eV and 0.18 eV, respectively, which is nearly perfect for HER. However, at the higher coverage ($\theta = 4/6$ or higher), the rather positive ΔG_{H^*} indicates that the H atoms are difficult to absorb on the P sites, making the ML-PC unsuitable for HER. The above results suggest that the ML-PC have high catalytic activity for HER at a moderate hydrogen coverage.

Similarly, the overall ΔG_{H^*} of BL-PC shows an upward trend from -0.14 eV to 1.62 eV with the coverage increasing from $\theta = 1/12$ to $\theta = 12/12$. It is worth noting that the ΔG_{H^*} is 0.13 eV at the coverage of $\theta = 3/12$, which makes BL-PC proper for HER. But for the coverage higher than $\theta = 6/12$, the values of free energy exceed 0.43 eV, demonstrating a weakened bond between H atom and P sites. Corresponding to ML-PC, the evolution of ΔG_{H^*} at different hydrogen coverage reveals the high catalytic activity of BL-PC at relatively low coverage. Moreover, the band structure of BL-PC under different coverage are calculated and shown in Fig. A2. The results show that under the H coverage of 1/12, 3/12, 9/12, and 12/12, the band structures of BL-PC show a metallic property, whereas under the H coverage of 6/12, the BL-PC is a semiconductor with bandgap of 1.24 eV, as shown in Fig. A2(c).

In reality, the fabrication of 2D materials usually needs a certain substrate to grow on. Therefore, as illustrated in Figs. 5(a1) and 5(b1), the hybrid structures of ML-PC (BL-PC) and graphene (G) are constructed to examine the influence of graphene substrate on the HER activity. After fully structure optimization, the lattice parameter of ML-PC@G (BL-PC@G) is 9.95 Å (9.98 Å). Furthermore, the mismatch for ML-PC is -0.9% and that for BL-PC is -1.25%, demonstrating that an external strain is imposed after composing the ML-PC (BL-PC) with graphene. The stability of hybrid structures is examined next by computing the cohesive energy: $E_{coh} = E_{tot} - E_{PC} - E_G$, where E_{tot}, E_{PC}, E_G represent the total energy of hybrid structures, the energy of PC, and the energy of graphene, respectively. The cohesive energy of ML-PC@G and BL-PC@G are -0.26 eV and -1.64 eV, respectively, which verifies the hybrid structures composed of PC and G are thermodynamically stable.

As shown in Fig. 5(a2), in the ML-PC@G hybrid system, the ΔG_{H^*} value of P site changes from -0.05 eV to -0.14 eV, which remains comparable to Pt-based catalyst. Nevertheless, the ΔG_{H^*} value of C site becomes more negative (-0.52 eV to -0.76 eV) meaning the interaction between the H atom and C site is stronger. Correspondingly, the effect of the graphene substrate on the intrinsic activity of BL-PC is depicted in Fig. 5(b2). The free energy of the 4-co-P site is optimized to 0.16 eV as BL-PC attaching with graphene substrate. Furthermore, the graphene has a slight effect on the activity of 3-co-P site on BL-PC, due to the ΔG_{H^*} of 3-co-P site decreases from -0.14 eV to -0.19 eV. Thus, the graphene substrate can affect the activity of BL-PC positively and barely influence that of ML-PC.

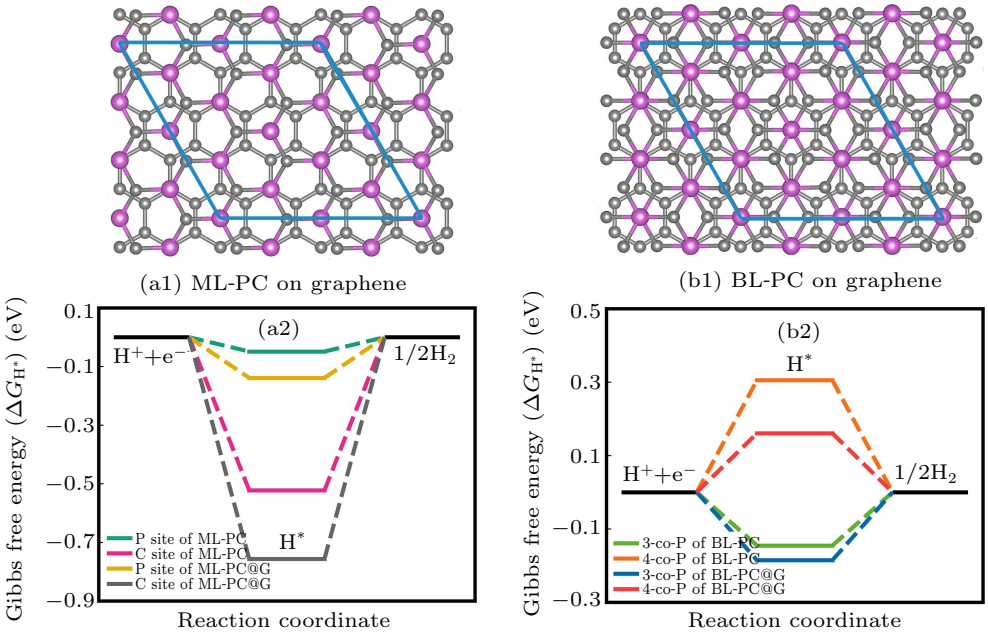


Fig. 5. Optimized geometric structure and computed free energy diagram of (a) monolayer PC and (b) bilayer PC on graphene substrate.

The change of ΔG_{H^*} value of layered PC on graphene substrate can be attributed to the electronic structure, thus the partial density of states (PDOS) of ML-PC@G and BL-PC@G is studied and shown in Fig. 6. The key properties of ML-PC are well preserved in PDOS of ML-PC@G, where the p orbitals of P and C atoms play an important role in the metallic property. Correspondingly, in the PDOS of BL-PC@G, the semiconductor properties of BL-PC are retained and the electronic states near Fermi level are contributed by graphene substrate, which could significantly enhance the electric conductivity and promote the electrocatalytic activity.

The interaction between layered PC and graphene substrate can be characterized by the charge transfer between the ML-PC (BL-PC) and the graphene substrate. Based on Bader charge analysis, in the PC@G system, 0.02 e is transferred from the graphene substrate to ML-PC, which could signif-

icantly enhance the electric conductivity. Moreover, the H atom adsorbed on P site gains 0.387 *e*, more than the charge of 0.373 *e* on the P site of pristine ML-PC, rendering a more negative ΔG_{H^*} value of ML-PC on the graphene substrate. Besides, it is intriguing that the charge transfer between BL-PC and graphene substrate is not same as H atom adsorbing on different sites. When an H atom adsorbs on the 3-co-P site of BL-PC, the charge of 0.012 *e* is transferred from graphene to BL-PC and the H atom gains 0.382 *e* from the 3-co-P site, less than the charge of 0.404 *e* of free-standing BL-PC. When an H atom absorbs on the 4-co-P site, however, the charge of 0.0003 *e* is transferred from graphene to BL-PC, meaning a weaker interaction between BL-PC and graphene substrate. The transferred charge between H atom and 4-co-P site of BL-PC@G (0.38 *e*) is less than that of free-standing BL-PC (0.53 *e*), illustrating a positive effect of graphene substrate on the electrocatalytic activity of 4-co-P site of BL-PC. Therefore, for the same active site, the less charge transfer to the H atom, the closer to zero the GH^* is, demonstrating a higher HER performance.

In the presence of an adsorbed hydrogen atom, the differential charge density of ML-PC@G and BL-PC@G is studied to analyze the charge distribution in these two systems. The amounts of electron transfer can be visualized by the three-dimensional (3D) differential charge density, defined as $\Delta\rho = \rho_{\text{total}} - \rho_{\text{H}} - \rho_{\text{PC@G}}$, where ρ_{total}, ρ_{H}, and $\rho_{\text{PC+G}}$ stand for the charge density of the hybrid system, isolated H atom, and PC@graphene, respectively. The 3D differential charge density of ML-PC@G and BL-PC@G with an H tom is shown in Fig. 7, respectively, where the yellow (blue) region represents the charge accumulation (depletion). The yellow region is mainly distributed around the absorbed H atom and the blue region mainly around the P atom, further indicating the charge transfer mainly happens between the H and P sites. Above all, the change of coordination system and moderate external strain could effectively optimize the HER catalytic activity of the 2D PC sheet and the 2D PC-based materials can be promising candidates for highly efficient HER electrocatalyst.

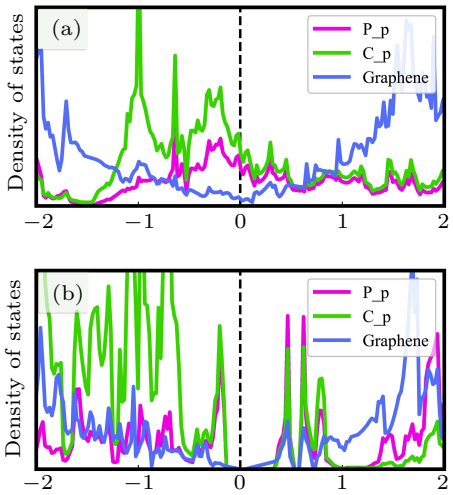


Fig. 6. Partial density of states (PDOS) of (a) ml-PC and (b) bl-PC on graphene. The Fermi level is shifted to zero.

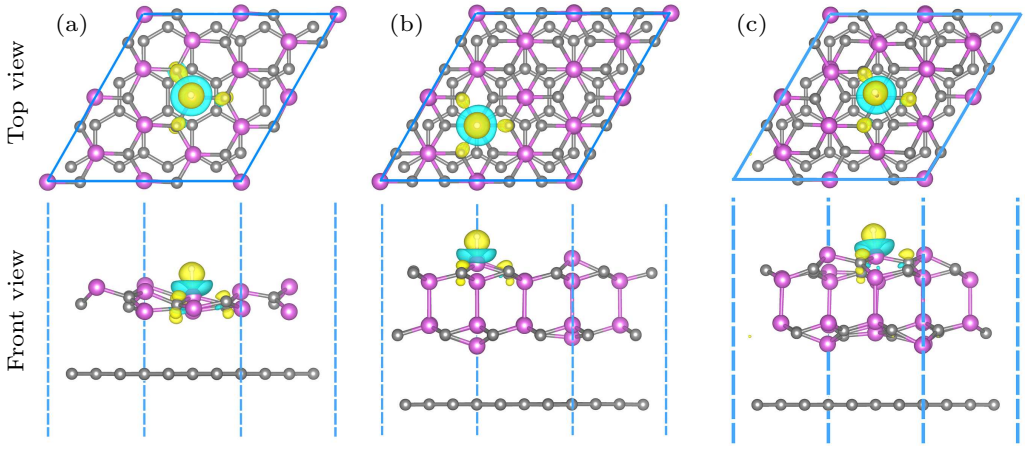


Fig. 7. Differential charge density of (a) P site of ml-PC on graphene, (b) 3-coordinated-P site and (c) 4-co-P site of bl-PC on graphene. The yellow and blue regions represent charge accumulation and depletion, respectively. The iso-surface value is set to 0.005/Å.

4. Summary

In summary, the catalytic activity of pristine ML-PC and BL-PC with the 3-co-P site and 4-co-P site are systematically investigated and the effect of external strain and interfacial engineering on the HER performance is examined via DFT calculation. The calculated ΔG_{H^*} values indicate that P site is more active for HER than C site in ML-PC. For the BL-PC, the activity of 4-co-P site is lower than that of 3-co-P site, which is comparable to P site in ML-PC. Interestingly, applying external strain could optimize the ΔG_{H^*} of the 4-co-P site closer to zero and enhance the overall HER activity of BL-PC. Additionally, the results of the free energy of ML-PC and BL-PC at different coverage show that both layered PC materials exhibit high catalytic activity at relatively low coverage. The effect of the graphene substrate on HER activity of ML-PC and BL-PC is further analyzed and the activity of P-site in ML-PC and

3-co-P site in BL-PC is insensitive to the graphene substrate, whereas the activity of 4-co-P is significantly enhanced by attaching the BL-PC to graphene, which can be understood by the interaction between BL-PC and graphene. All these fascinating results illustrate a promising strategy of changing the configuration system to enhance the intrinsic catalytic activity and the 2D layered PC-based materials are ideal and promising electrocatalyst for HER.

Appendix A: Supporting information

In order to better understand and explain the descriptions in the main text, the following figures are given below for references.

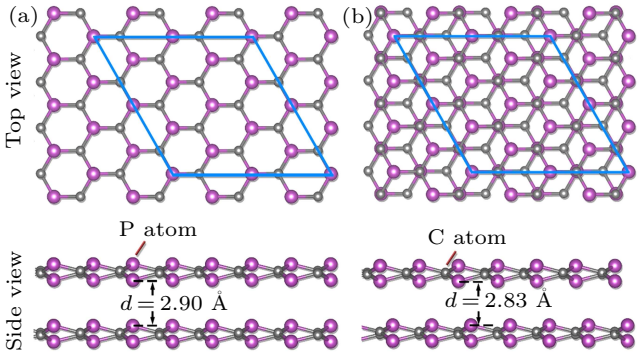


Fig. A1. Optimized atomic configuration of (a) P–P stacking vdW bilayer P–C structure and (b) P–C stacking bilayer PC structure. The blue rhomb represents the redefined cell. The P and C atoms are denoted as pink and gray spheres, respectively. The equilibrium distance between two layers is represented by d.

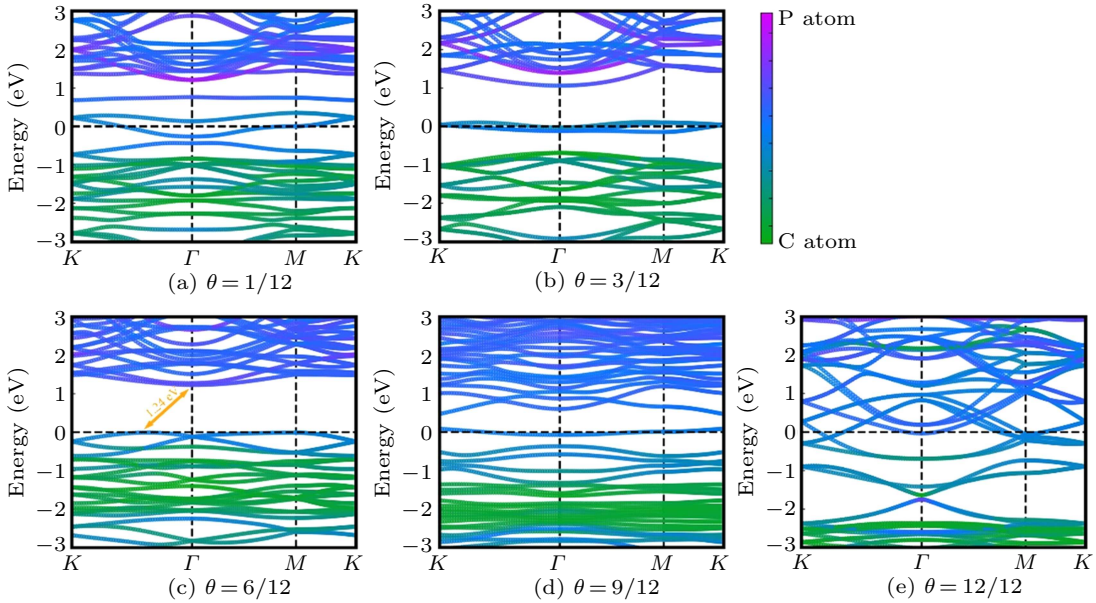


Fig. A2. (a)–(e) Band structures of bilayer PC under different H coverages. The Fermi level is set to zero.

References

[1] Dresselhaus M S and Thomas I L 2001 *Nature* **414** 332
[2] Dunn S 2002 *Int. J. Hydrog. Energy* **27** 235
[3] Norskov J K, Bligaard T, Logadottir A, Kitchin J R, Chen J G, Pandelov S and Norskov J K 2005 *J. Electrochem. Soc.* **152** J23
[4] Schlapbach L and Zuttel A 2001 *Nature* **414** 353
[5] Strmcnik D, Uchimura M, Wang C, Subbaraman R, Danilovic N, van der Vliet D, Paulikas A P, Stamenkovic V R and Markovic N M 2013 *Nat. Chem.* **5** 300
[6] Jiao Y, Zheng Y, Jaroniec M and Qiao S Z 2015 *Chem. Soc. Rev.* **44** 2060
[7] Greeley J, Jaramillo T F, Bonde J, Chorkendorff I B and Norskov J K 2006 *Nat. Mater.* **5** 909
[8] Wang P, Jiang K, Wang G, Yao J and Huang X 2016 *Angew. Chem. Int. Edit.* **55** 12859
[9] Zheng Y, Jiao Y, Jaroniec M and Qiao S Z 2015 *Angew. Chem. Int. Edit.* **54** 52
[10] Zheng S, Yu T, Lin J, Lou H, Xu H and Yang G 2019 *J. Mater. Chem. A* **7** 25665
[11] Lin X D and Zhou Y G 2019 *J. Phys.: Condens. Matter* **31** 355302
[12] Zhang B, Zhou J, Guo Z, Peng Q and Sun Z 2020 *Appl. Surf. Sci.* **500** 144248
[13] Yu Q, Luo Y, Qiu S, Li Q, Cai Z, Zhang Z, Liu J, Sun C and Liu B 2019 *ACS Nano* **13** 11874
[14] Lei B, Zhang Y Y and Du S X 2020 *Chin. Phys. B* **29** 058104
[15] Zhang J, Jiang W J, Niu S, Zhang H T, Liu J, Li H Y, Huang G F, Jiang L, Huang W Q, Hu J S and Hu W P 2020 *Adv. Mater.* **32** 9
[16] Chen Y, Yang K, Jiang B, Li J, Zeng M and Fu L 2017 *J. Mater. Chem. A* **5** 8187
[17] Karmodak N and Andreussi O 2020 *Acs Energy Lett.* **5** 885
[18] Gao G, O'Mullane A P and Du A 2016 *ACS Catal.* **7** 494
[19] Chaudhari N K, Jin H, Kim B, Baek D S, Joo S H and Lee K 2017 *J. Mater. Chem. A* **5** 24564
[20] Zhang C, Yu G, Ku R, Huang X and Chen W 2019 *Appl. Surf. Sci.* **481** 272
[21] Wu H H, Huang H, Zhong J, Yu S, Zhang Q and Zeng X C 2019 *Nanoscale* **11** 12210
[22] Zhang R, Yu G, Gao Y, Huang X and Chen W 2020 *Inorg. Chem. Front.* **7** 647
[23] Zhao N, Wang L, Zhang Z and Li Y 2019 *ACS Appl. Mater. Inter.* **11** 42014
[24] Sharma M D, Mahala C and Basu M 2020 *Inorg. Chem.* **59** 4377
[25] Zhao X, He D W, Wang Y S and Fu C 2018 *Chin. Phys. B* **27** 068103
[26] Silva J L, Brena B and Araujo C M 2020 *J. Phys. Chem. C* **124** 8726
[27] Riyajuddin S, Aziz S K T, Kumar S, Nessim G D and Ghosh K 2020 *Chemcatchem* **12** 1394
[28] Li Y Y, Si Y, Han E X, Huang W Q, Hu W Y, Pan A L, Fan X X and Huang G F 2019 *J. Phys. D: Appl. Phys.* **52** 105502

[29] Li Y Y, Si Y, Zhou B X, Huang W Q, Hu W, Pan A, Fan X and Huang G F 2019 *Nanoscale* **11** 16393
[30] Yu S, Rao Y C, Wu H H and Duan X M 2018 *Phys. Chem. Chem. Phys.* **20** 27970
[31] Zhang X, Chen A, Zhang Z, Jiao M and Zhou Z 2018 *J. Mater. Chem. A* **6** 11446
[32] Zhang X L, Yang Z X, Yang X, Wang Y L and Lu Z S 2018 *Int. J. Hydrog. Energy* **43** 20573
[33] Lu J, Zhang X, Liu D N, Yang N, Huang H, Jin S W, Wang J H, Chu P K and Yu X F 2019 *ACS Appl. Mater. Inter.* **11** 37787
[34] Gan Y, Xue X X, Jiang X X, Xu Z, Chen K, Yu J F and Feng Y 2019 *J. Phys.: Condens. Matter* **32** 025202
[35] Rajbanshi B and Sarkar P 2017 *J. Phys. Chem. Lett.* **8** 747
[36] Blochl 1994 *Phys. Rev. B* **50** 17953
[37] Perdew J P, Burke K and Ernzerhof M 1996 *Phys. Rev. Lett.* **77** 3865
[38] Kresse G and Furthmuller J 1996 *Comp. Mater. Sci.* **6** 15
[39] Grimme S, Ehrlich S and Goerigk L 2011 *J. Comput. Chem.* **32** 1456
[40] Grimme S, Antony J, Ehrlich S and Krieg H 2010 *J. Chem. Phys.* **132** 154104
[41] Huang T, Chen Q, Cheng M Q, Huang W Q, Hu W Y and Huang G F 2019 *J. Phys. D: Appl. Phys.* **52** 7
[42] Chianelli R R, Berhault G, Raybaud P, Kasztelan S, Hafner J and Toulhoat H 2002 *Appl. Catal. a-Gen.* **227** 83
[43] Medford A J, Vojvodic A, Hummelshoj J S, Voss J, Abild-Pedersen F, Studt F, Bligaard T, Nilsson A and Norskov J K 2015 *J. Catal.* **328** 36
[44] Gao G, Sun G and Du A 2016 *J. Phys. Chem. C* **120** 16761
[45] Huang T, Lian J C, Yang K, Si Y, Wu H Y, Huang W Q, Hu W Y and Huang G F 2020 *Physica E* **118** 113962